Article

Synthesis, Characterization and Conformational Analysis of Two Novel 4(1*H*)-Quinolinones

Lidiane J. Michelini, [a,b] Wesley F. Vaz,[c] Luiz F. N. Naves,[c] Caridad N. Pérez[a] and
Hamilton B. Napolitano *,c,d

aInstituto de Química, Universidade Federal de Goiás, 74690-900 Goiânia-GO, Brazil

bInstituto Federal de Ciência, Educação e Tecnologia Goiano, 76200-000 Iporá-GO, Brazil

cCiências Exatas e Tecnológicas, Universidade Estadual de Goiás, 75132-903 Anápolis-GO, Brazil

*dLaboratório de Novos Materiais, Centro Universitário de Anápolis,
75083-515 Anápolis-GO, Brazil*

Quinolinones are a class of organic compounds known as alkaloids found in several plants and also can be synthesized. Their large use in therapies regards their wide biological potential like antitumor, psychiatric and neurological agents. Two substances were structurally characterized: (*E*)-3-(2-nitrobenzylidene)-2-(4-methoxyphenyl)-1-(phenylsulfonyl)-2,3-dihydroquinolin-4(1*H*)-one (NMQ), and (*E*)-3-(2-chlorobenzylidene)-2-(2-methoxyphenyl)-1-(phenylsulfonyl)-2,3-dihydroquinolin-4(1*H*)-one (CMQ). These compounds were synthesized, crystallized, characterized by single crystal X-ray diffraction and theoretical calculations. The NMQ and CMQ crystals are formed by a pair of enantiomers and crystallized in the centrosymmetric group P21/c with similar volume and density. Differences noted on crystal packing and supramolecular arrangement are associated to substituent group chlorine in CMQ and nitro in NMQ. The calculated infrared (IR) spectra show a good agreement with experimental values. The highest occupied molecular orbital (HOMO) and lowest unoccupied molecular orbital (LUMO) energies show CMQ more kinetically stable with a higher resistance to transfer charge than NMQ.

Keywords: quinolinones, X-ray diffraction, theoretical analysis

Introduction

Organic compounds known as quinolinones alkaloids are found in several plants and have been used as remedies since ancient times.[1] The 4(1*H*)-quinolinones are a class of these compounds that occurs naturally in the environment and also can be synthesized.[2,3] Their application is largely known as antibiotic in the treatment of infection,[4] but other studies have shown that these compounds may be used in many areas, for example, in medicine with different biological potential uses,[5-11] like antitumor[12,13] or psychiatric and neurological agents[14] or in engineering by their photophysical properties.[15] For a better understanding of where and how these substances may be used, the structural investigation is a significant tool. It provides a complete knowledge of the molecular structure embracing the atomic architecture, molecular conformation and crystal packing.

Owing this information, it is possible to open new frontiers, including the development of novel materials and drugs.[16] This sort of analysis is largely applied for the acquaintance of quinolinones providing, for example, information about the relationship between structure and activity in biological tests.[17,18]

With the aim to obtain structural information of novel 4(1*H*)-quinolinones, two substances were analyzed: (*E*)-3-(2-nitrobenzylidene)-2-(4-methoxyphenyl)-1-(phenylsulfonyl)-2,3-dihydroquinolin-4(1*H*)-one (NMQ), and (*E*)-3-(2-chlorobenzylidene)-2-(2-methoxyphenyl)-1-(phenylsulfonyl)-2,3-dihydroquinolin-4(1*H*)-one (CMQ). Thus, the purpose is the structural elucidation throughout the single crystal X-ray diffraction methodology, encompassing crystalline arrangement, interatomic distance and angles, molecular geometry, inter and supramolecular interactions and Hirshfeld surface analysis. In this aspect, this work provides important information for future studies and applications of the 4-(1*H*)-quinolinones.

*e-mail: hbnapolitano@gmail.com

Experimental

Synthesis and crystallization

NMQ (**5**) and CMQ (**6**) were obtained from sulfonamide chalcones **1** and **2**, and reacted with benzaldehydes **3** and **4** (2:1), respectively (Scheme 1), in alkaline reaction environmental for 24 h. The resulting precipitates **5** and **6** were purified by multi-solvent slow recrystallization from dichloromethane (CH_2Cl_2) and ethanol (CH_3CH_2OH) (4:1), after drying at room temperature.

Crystallographic characterization

A radiation of graphite monochromated MoKα with a wavelength of 0.71073 Å, at room temperature, was focused in a single crystal of NMQ and CMQ using a Bruker Apex II CCD diffractometer. This was executed to collect the diffraction data. Right after, this data were processed utilizing the Bruker program APEX2,[19] choosing the direct methods as the option for the structure solution. The software SHELX2016[20] was employed for the refinement, opting for the least square methods. For the positioning and calculation of the hydrogen atoms, the refinement was fixed with individual displacement parameter [Uiso(H) = 1.2 Ueq or 1.5 Ueq], using 0.97 Å as the lengths of C–H for aromatic groups, and 0.97 Å for methyl groups. Structural information described in tables, figures and molecular representations were made using the softwares WinGX,[21] Ortep[21] and Mercury,[22] respectively. The PLATON[23] program was also utilized to verify the possible interactions involving hydrogen bonds.

Hirshfeld surface analysis

To measure the intermolecular interactions in the crystal arrangement of NMQ and CMQ, Crystal Explorer 3.1 software[24,25] was selected as a tool of Hirshfeld surface (HS) analysis. Due to this, the graphical representation of the normalized contact distances (d_{norm}), shape index and 2D fingerprint plot of both compounds was possible. To represent the HS, it was used a diagram that illustrated the molecular interactions with different grades, which change according to the atoms and connections types on the surface of the molecule.[26] It allows a visualization and a better understanding about which interaction is more and less significant for the crystal packing.[27] The base to generate an HS is to branch the space in regions according to electronic distribution engendering the weighting function W(r), which corresponds to the value of 0.5. In this equation,[25] the sum of the electronic contribution of part of the molecule overlaps the contribution of all the crystal, represented by:

$$W(r) = \frac{\rho_{molecule}(r)}{\rho_{crystal}(r)} \qquad (1)$$

Meanwhile, when near contacts are present, it is possible to analyze using the distance function. It enables the formation of two regions in the intermolecular contact characterized by donation and acceptance properties and can be equated d_{norm}.[28]

$$d_{norm} = \frac{\left(d_i - r_i^{vdW}\right)}{r_i^{vdW}} + \frac{\left(d_e - r_e^{vdW}\right)}{r_e^{vdW}} \qquad (2)$$

The two regions compose the surface taking intern and extern atomic nucleus as references. The accept region (d_i) is the distance from an internal atom to HS, while the d_e region is equivalent to the donor region measuring from an external atomic nucleus until HS.[28] These two distances combined in a 2D graph, called fingerprint, give unique information about the contacts present in the structure.[25] Another useful appliance provided by HS is the recognition of hydrophobic interactions by means of shape index (S) analysis, which is a dimensionless qualitative measure of surface shape, defined in terms of principal curvatures κ_1 and κ_2 by the function:

$$S = \frac{2}{\pi} \arctan \frac{\kappa_1 + \kappa_2}{\kappa_1 - \kappa_2} \qquad (3)$$

(**1**): R_1 = *p*-CH$_3$
(**2**): R_1 = *o*-OCH$_3$

(**3**): R_2 = *o*-Cl
(**4**): R_2 = *o*-NO$_2$

(**5**): R_1 = *p*-CH$_3$; R_2 = *o*-NO$_2$
(**6**): R_1 = *o*-OCH$_3$; R_2 = Cl
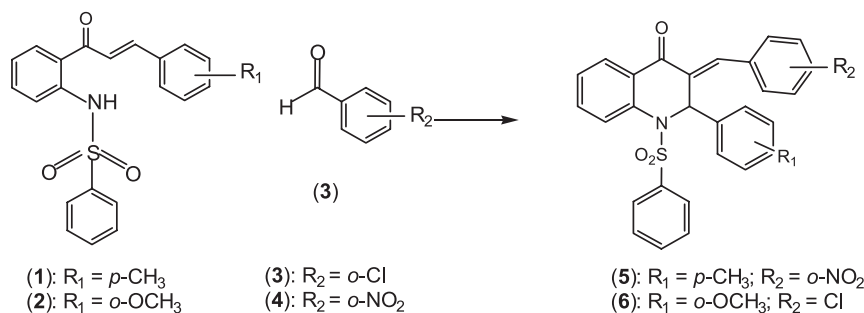
Scheme 1. Synthesis of NMQ (**5**) and CMQ (**6**).

Computational details

Theoretical calculations, at density functional theory (DFT) methods, were done with Gaussian 09 package[29] to obtain the optimized geometry, vibrational wavenumbers and theoretical vibrational spectra of CMQ and NMQ. In the literature, M06-2X/6-311++G(d,p) method has been used to obtain vibrational frequencies[30-33] and have proved to be one of the best density functionals for non-covalent interactions.[34] In addition, there is already a scale factor calculated[35,36] for vibrational wavenumbers obtained using it. The starting geometries considered were those provided by the CIF file of each molecule. VEDA 4 program[37] and GaussView package[38] were used to obtain the suggested vibrational frequency assignments. To obtain more coherent values between theoretical and experimental wavenumbers, the vibrational frequencies were scaled using as scale factor[35] 0.9489. In general, the scale factor equation is represented by[39]

$$\varepsilon_{vib}^{G} \cong \frac{\hbar c}{2} \sum_{m} \left(\lambda \omega_{m} \right) \qquad (4)$$

where ε_{vib}^{G} is the harmonic approximation, ω_{m} is the computed harmonic vibrational frequency of mode m in

wavenumber, $\hbar$ is Planck's constant. The scale factor is the constant λ.

The frontier molecular orbitals (FMO) and molecular electrostatic potential map (MEP) calculations were performed at same level of theory and, to comprehend reactional aspects of these molecules, the HOMO-LUMO energy gap, softness and hardness were obtained, as previously described.[40]

Results and Discussion

Solid state characterization

The molecule NMQ possesses a *p*-methoxyphenyl group connected to the chiral center C10 and an *o*-nitrobenzylidene group connected to a α-β insaturation in relation to ketone. A similar pattern occurs with the molecule CMQ, which has an *o*-methoxyphenyl group connect at atom C10 and an *o*-chlorobenzylidene group connected to ketonic ring. Both molecules have a phenylsulfonyl group connected to the nitrogen present in the heterocyclic ring of the quinolinone, constituting a backbone together with the benzene ring connected to C5 and C6 atoms. The NMQ and CMQ crystals are formed
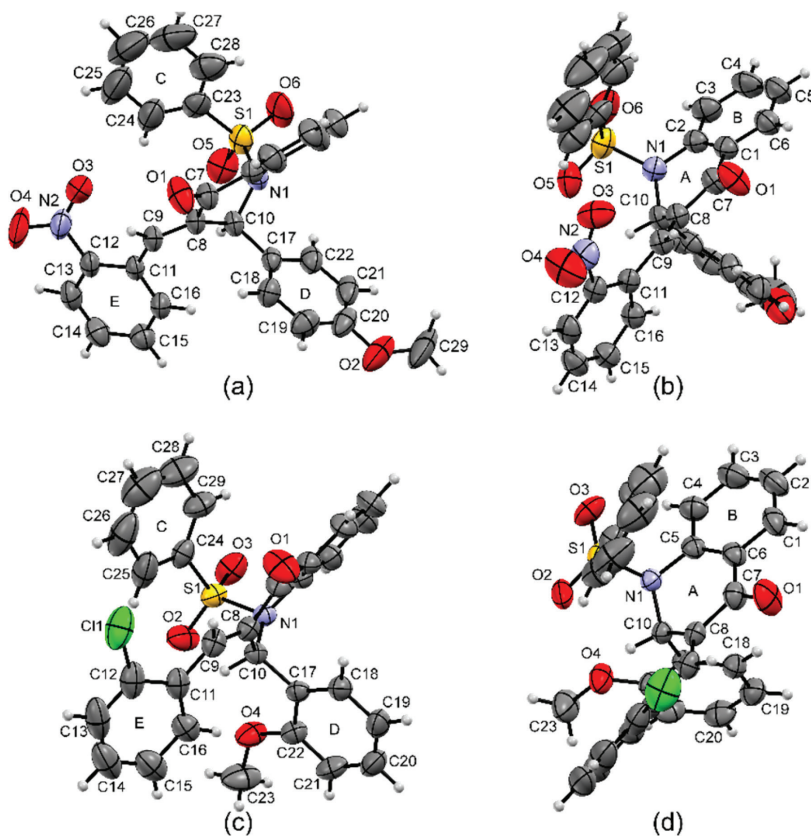
Figure 1. Ortep representation of the asymmetric units with 50% probability of NMQ (a, b) and CMQ (c, d) from two perspectives.

by a pair of enantiomers that have a chiral center located at carbon 10 (Figure 1). Both molecules crystallized in the centrosymmetric group P21/c with one molecule in the asymmetric unit, and for molecules at the unit cell. Figure 1 shows the Ortep representation of the *R*-enantiomer, arbitrarily chosen as asymmetric unit. The resume of crystallographic information of the analyzed compounds is described in Table 1. The intermolecular interactions data for NMQ are shown in Table 2.

Interactions of the type C−H···π and π···π were also identified as non-classical interactions and are described in Table 3. The non-classical interactions are indicated on Figure 2.

There is a bifurcated interaction C15−H15···O4 and C29−H29B···O4 which forms a line of molecules in the direction of c axis, alternating between R and S enantiomers, as shown in Figure 3. Figure 3 also shows how these lines are interconnected by the contacts C13−H13···O6, forming a layer along the plane $\overrightarrow{(ac)}$. Each layer interacts with its inverse layer by means of the dimers formed by the contact C9−H9···O1 (Figure 4). The structure occurs by stacking these pairs of layers in the direction of b axis. Figure 4 shows the packaging of the crystal.

From the graphical analysis of NMQ HS, it was verified that the most dominant interactions correspond to the contacts C13−H13···O6 and C15−H15···O4. The other

Table 1. Refinement, structure and crystal data for the compounds NMQ and CMQ

	NMQ	CMQ
Empirical formula	$C_{29}H_{23}N_2O_6S$	$C_{29}H_{23}ClN_1O_4S$
Formula weight / (g mol^{-1})	527.6	515.98
Temperature / K	296 (2)	296 (2)
Crystal system, space group	monoclinic, P 21/c	monoclinic, P 21/c
Unit cell dimensions	a = 9.4515(9) Å	a = 11.2257(7) Å
	b = 19.3086(16) Å	b = 10.4938(5) Å
	c = 14.5216(12) Å	c = 21.4824(12) Å
	β = 102.448(3)°	β = 95.295(2)°
Volume / Å^3	2587.82	2519.8(2)
Z, calculated density	4, 1.35 g cm^{-3}	4, 1.360 mg m^{-3}
Absorption coefficient / mm^{-1}	0.172	1.859
F (000)	1100.0	1072
Cell measurement theta / degree	1.8 to 25.0	1.82 to 26.43
hkl indices	$-10 \leq h \leq 11$	$-14 \leq h \leq 13$
	$-22 \leq k \leq 22$	$-13 \leq k \leq 13$
	$-17 \leq l \leq 17$	$-26 \leq l \leq 25$
Reflections collected / independent	87505/5296	29845/4019
Refinement method	min square F^2	min square F^2
Goodness-of-fit (goof)	1.122	1.058
Final indices R [I > 2 (I)]	R_1 = 0.0442	R_1 = 0.0517
	wR_2 = 0.114	Rw_2 = 0.1439
R indices (all data)	R_1 = 0.0564	R_1 = 0.0673
	wR_2 = 0.130	Rw_2 = 0.1578

NMQ: (*E*)-3-(2-nitrobenzylidene)-2-(4-methoxyphenyl)-1-(phenylsulfonyl)-2,3-dihydroquinolin-4(1*H*)-one; CMQ: (*E*)-3-(2-chlorobenzylidene)-2-(2-methoxyphenyl)-1-(phenylsulfonyl)-2,3-dihydroquinolin-4(1*H*)-one.

Table 2. Intermolecular interactions of NMQ, with distances and angles between the donor atom, hydrogen and acceptor atom

Code	D–H···A	d_{D-H} / Å	$d_{H···A}$ / Å	$d_{D···A}$ / Å	$\theta_{D-H···A}$ / degree	Symmetry code
			NMQ			
1N	C15−H15···O4	0.966	2.527	3.126	120.18	x, 1.5 − y, −1/2 + z
2N	C13−H13···O6	0.974	2.358	3.130	135.73	−1 + x, 1.5 − y, −1/2 + z
3N	C29−H29B···O4	0.921	2.701	3.271	120.88	x, y, −1 + z
4N	C9−H9···O1	0.954	2.676	3.519	147.80	1 − x, 1 − y, 2 − z

NMQ: (*E*)-3-(2-nitrobenzylidene)-2-(4-methoxyphenyl)-1-(phenylsulfonyl)-2,3-dihydroquinolin-4(1*H*)-one; D: donor atom; A: acceptor atom; d: distance; θ: angle.

Table 3. NMQ non-classical interactions C–H···π and π···π

Code	Intercation	Symmetry code
	NMQ	
5N	C26–H26···C_g1	– x, 1 – y, 2 – z
6N	C_g2···C_g3	–1 + x, y, z

NMQ: (*E*)-3-(2-nitrobenzylidene)-2-(4-methoxyphenyl)-1-(phenylsulfonyl)-2,3-dihydroquinolin-4(1*H*)-one.

interactions can be considered secondary, including the dimer formed by the contact C9–H9···O1. It was probably due to the approximation caused by the packing, as well as the contact C29–H29B···O4, as they are not evidenced by the characteristic color of the most intense contacts, as shown in Figure 5.

With the Hirshfeld surface, it was possible to confirm some secondary interactions, such as C26–H26···Cg1 and Cg2···Cg3 (Figure 6).

Table 4 summarizes the non-classical and intermolecular interactions of CMQ.

There is a bifurcated interaction C2–H2···O3 and C20-H20···O3 which forms a line of molecules in the direction $\overrightarrow{(ab)}$, and as also happens with NMQ bifurcated interactions, C2–H2···O3 and C20–H20···O3 alternated between R and S enantiomers, forming a centrosymmetric interaction. Between these inverse layers occurs an interaction provided by the dimer C15–H15···O2 (Figure 7).

The only non-classical interaction that occurs in CMQ molecule is centrosymmetric and it is between C14–H14 atoms and Cg1 ring forming a layer that stabilized the packing in $\overrightarrow{(ac)}$ direction, illustrated by Figure 8.

Figure 2. (a) NMQ non-classical interaction C26–H26···C_g1; (b) NMQ non-classical interaction C_g2···C_g3.
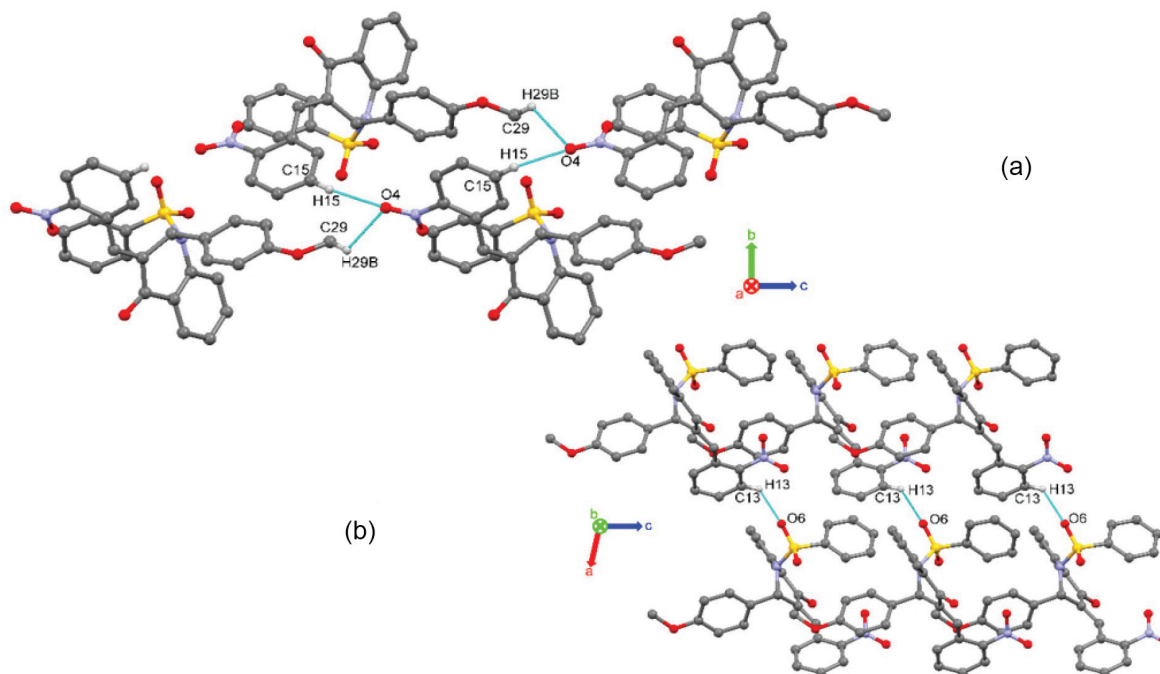
Figure 3. (a) NMQ chain of molecules formed by contacts C15–H15···O4 and C29–H29B···O4; (b) NMQ layer formed by the contacts C13–H13···O6.
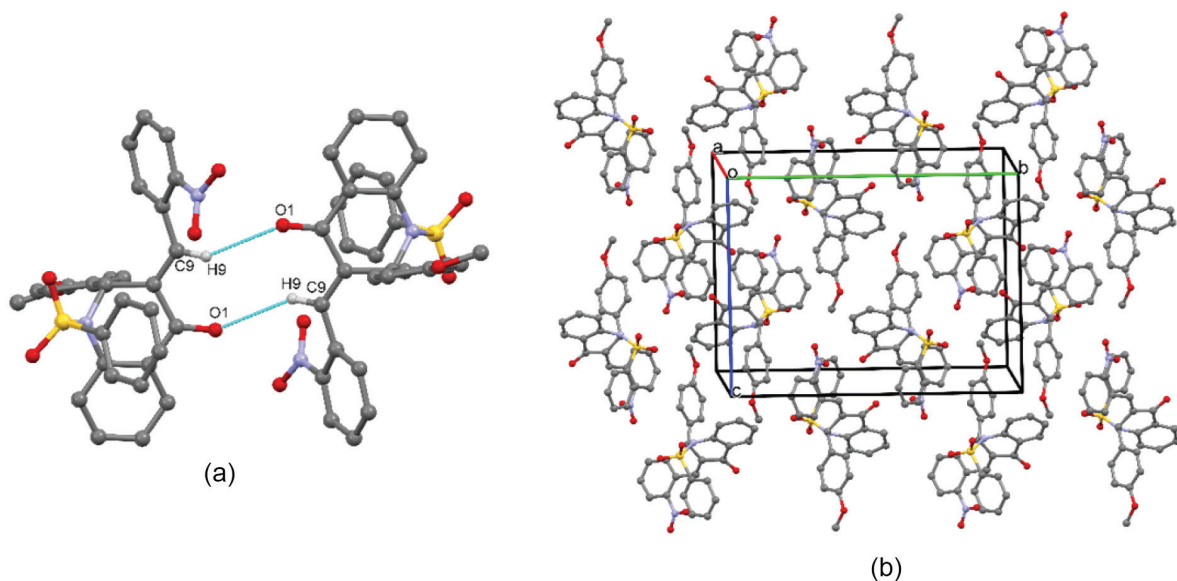
Figure 4. (a) NMQ dimer formed by interaction C9−H9···O1; (b) NMQ crystal packing.
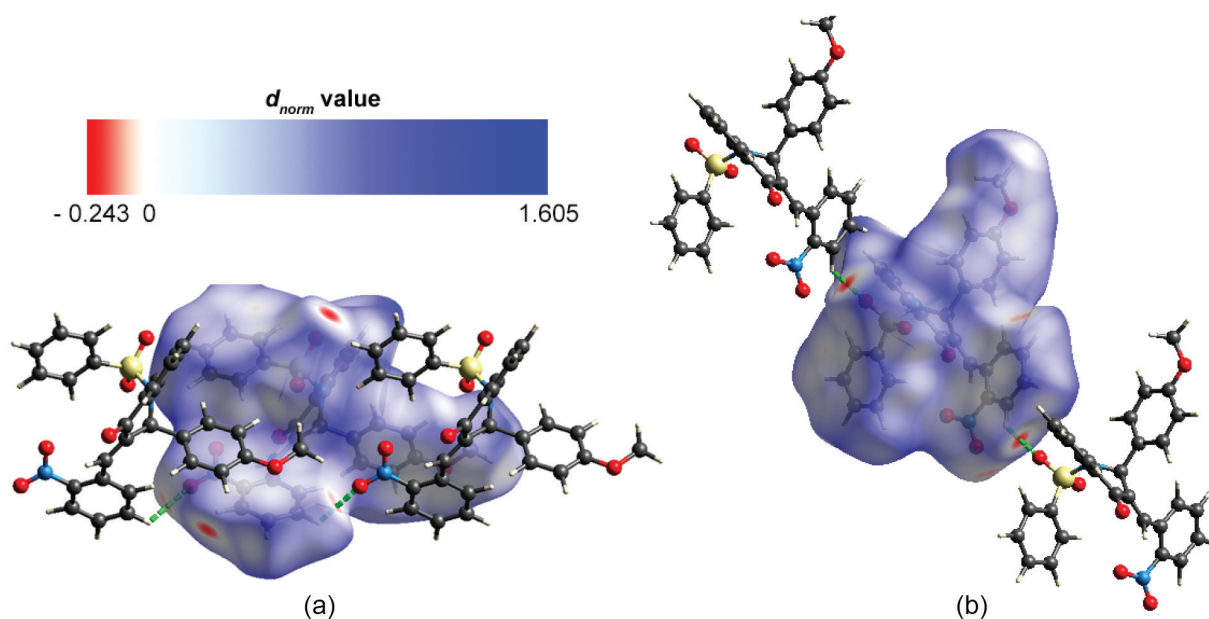
Figure 5. (a) Contact C15−H15···O4 evidenced by the red spot on HS; (b) contact C13−H13···O6 evidenced by the red spot on HS.

The CMQ structure occurs by stacking the layer formed by C2−H2···O3 and C14−H14···O3 in the direction of $\overrightarrow{(ac)}$ with the non-classical C14−H14···Cg1 and the dimer C15−H15···O2 forming chains between the layers. The Figure 9 shows the packaging of the CMQ crystal.

It was verified, as well as NMQ molecule, from the graphical analysis of HS from CMQ, that the most dominant interactions correspond to the contacts C2−H2···O3. After that, the dimer C15−H15···O2, contributes with 18.2% of the interactions of the system. The other bifurcated interaction can be considered secondary, C20−H20···O3, which was probably due to the

approximation caused by the packing as it is not evidenced by the characteristic color of the most intense contacts, as shown in Figure 10.

Unlike the NMQ molecule, when using the shape index analysis for CMQ, it was not noticeable π···π contacts, bought by the low percentage of C···C interactions indicating fingerprint with value of 3.6% and elevated distance (3.9 Å) between the rings of the sulfonyl group. Additionally, the non-classical interaction C14−H14··· Cg1 can be seen in Figure 11 contributing with 18% of the stabilizing packing system, proven by the fingerprint analysis.
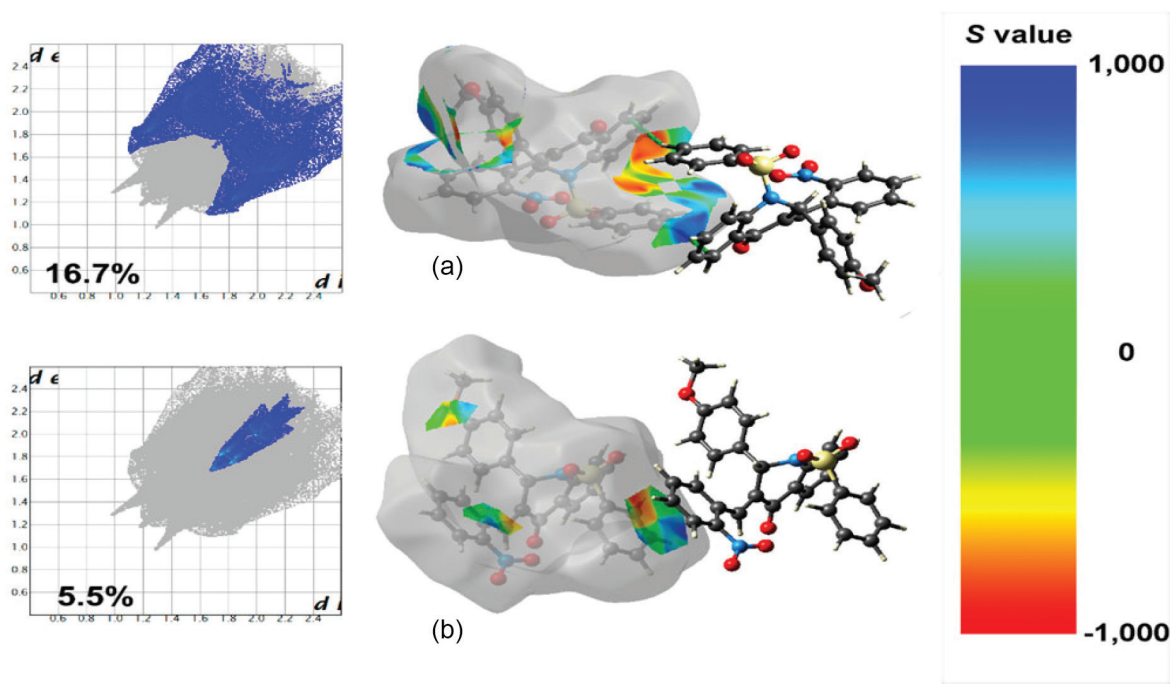
Figure 6. Fingerprint and Hirshfeld surface of the asymmetric unit revealing the contacts H···C (a) and C···C (b), including reciprocal contacts.

Table 4. Non-classical and intermolecular interactions of CMQ, with distances (d) and angles (θ) between the donor atom (D), hydrogen and acceptor atom (A)

Code	D–H···A	d_{D-H} / Å	$d_{H···A}$ / Å	$d_{D···A}$ / Å	$\theta_{D-H···A}$ / degree	Symmetry code
CMQ intermolecular interaction						
1C	C15–H15···O2	0.930	2.547	3.233	130.90	−x, 1 − y, 1 − z
2C	C2–H2···O3	0.930	2.444	3.350	164.67	1 − x, −1/2 + y, 1/2 − z
3C	C20–H20···O3	0.930	2.667	3.441	141.15	−x, −1/2 + y, 1/2 − z
CMQ non-classical intermolecular interaction						
Code	Interaction					Symmetry code
4C	C14–H14···Cg1					x, 1/2 − y, 1/2 + z

CMQ: (*E*)-3-(2-chlorobenzylidene)-2-(2-methoxyphenyl)-1-(phenylsulfonyl)-2,3-dihydroquinolin-4(1*H*)-one.

Theoretical analysis

In Table 5, the experimental and theoretical vibrational wavenumbers and theoretical infrared intensities are presented. The assignments presented show a good agreement between the theoretical scaled wavenumbers and the experimental values, thus, we expect reliability of the obtained band assignments. A brief discussion is given for vibrations of the main groups in CNQ and NMQ structures.

In the studied compounds, we have two types of double bonds between carbons; the first is found in the aromatic rings and the other in the vinyl group. For ν(C=C) in aromatic rings, bands are expected at 1600 to 1475 cm⁻¹ and for vinyl group, when conjugated with carbonyl group, between 1660 and 1600 cm⁻¹.[41] For CMQ, the ν(C=C) vibrations in aromatic rings are found at 1599 to 1463 cm⁻¹ and 1590 to 1551 cm⁻¹ in experimental and calculated spectra, respectively. On the other hand, for NMQ, these vibrational modes occur at 1607 to 1458 cm⁻¹ (experimental) and at 1601 to 1554 cm⁻¹ (calculated). The (C–C) stretching in vinyl group for CMQ is observed at 1599 cm⁻¹ in experimental spectra and calculated at 1623 cm⁻¹. In NMQ, these vibrations are assigned at 1607 and 1625 cm⁻¹, respectively.

The carbonyl group absorbs in the range from 1850 to 1650 cm⁻¹, but conjugation effects, such as those occurring in title compounds, result in a dropping of the (C=O) frequency.[41] The band at 1668 and at 1676 cm⁻¹, in IR spectrum, and the scaled frequencies at 1710 and 1714 cm⁻¹ are assigned to ν(C=O) vibration in CMQ and NMQ, respectively. For SO₂ group, in sulfonamide moiety, an
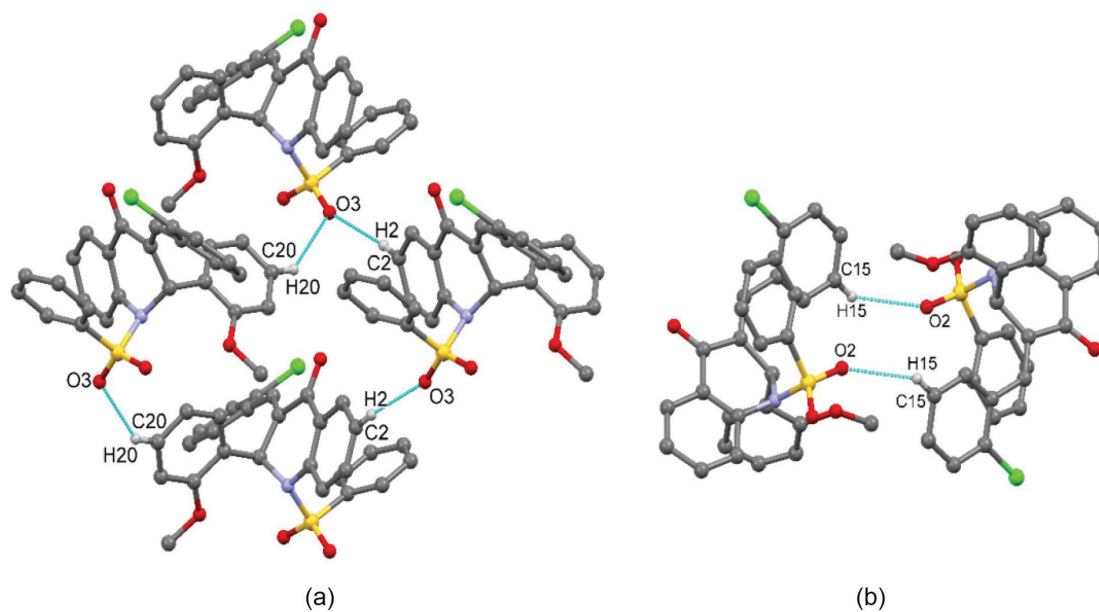
Figure 7. (a) CMQ chain of molecules formed by contacts C2−H2···O3 and C20−H20···O3 growing in the direction [110]; (b) CMQ dimer formed by interaction C15−H15···O2.
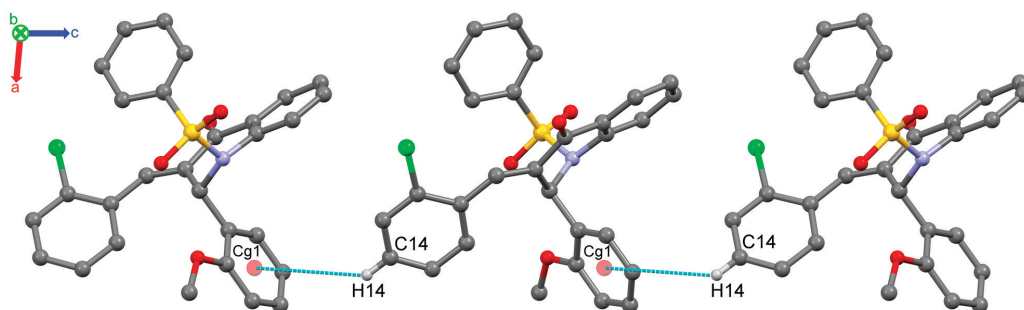
Figure 8. CMQ non-classical interaction C14−H14···Cg1 growing at [101] direction.
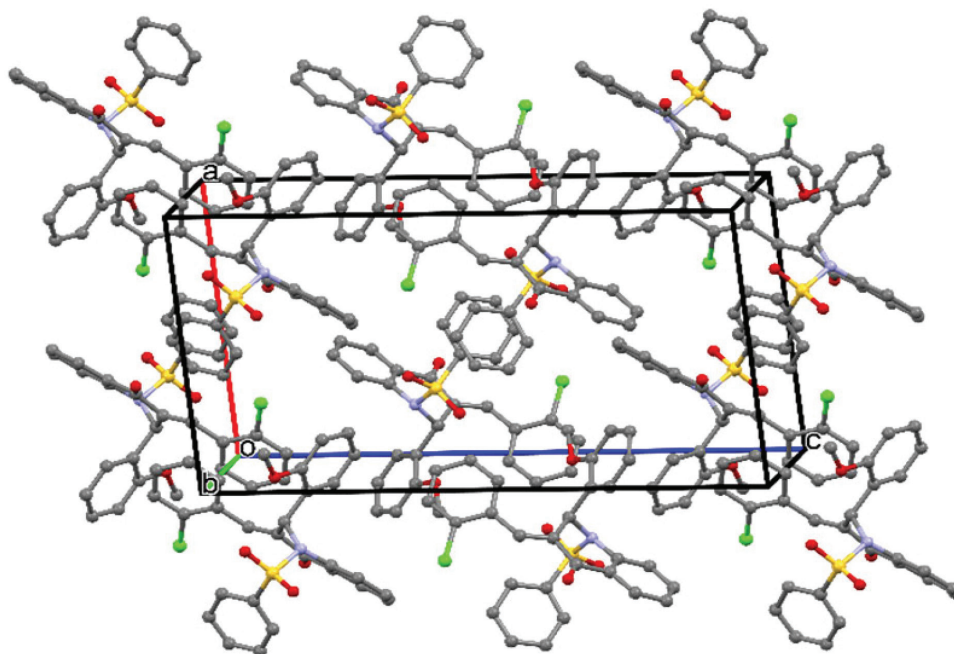
Figure 9. CMQ crystal packing.
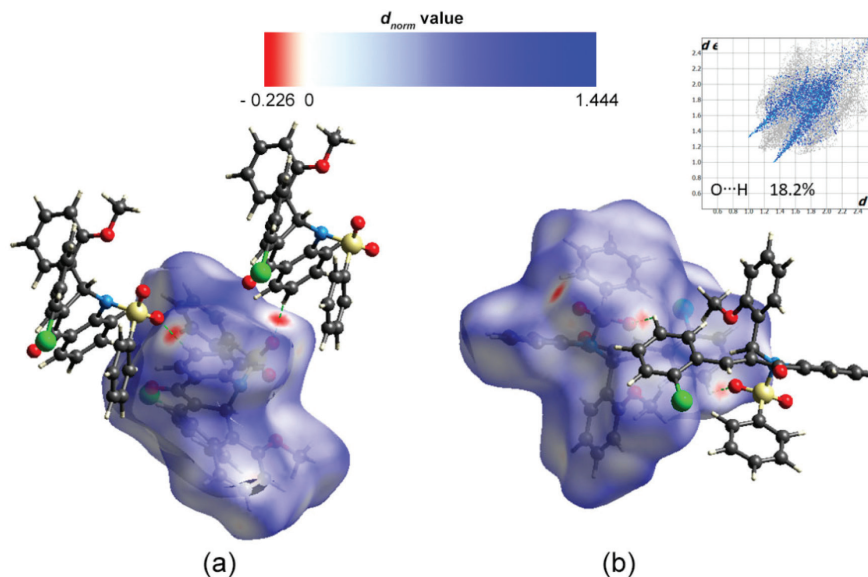
Figure 10. Hirshfield surface d_{norm} for CMQ molecule: (a) contact C2–H2···O3; (b) contact C15–H15···O2 evidenced by the red spots and fingerprint for O···H interactions including reciprocal contacts.
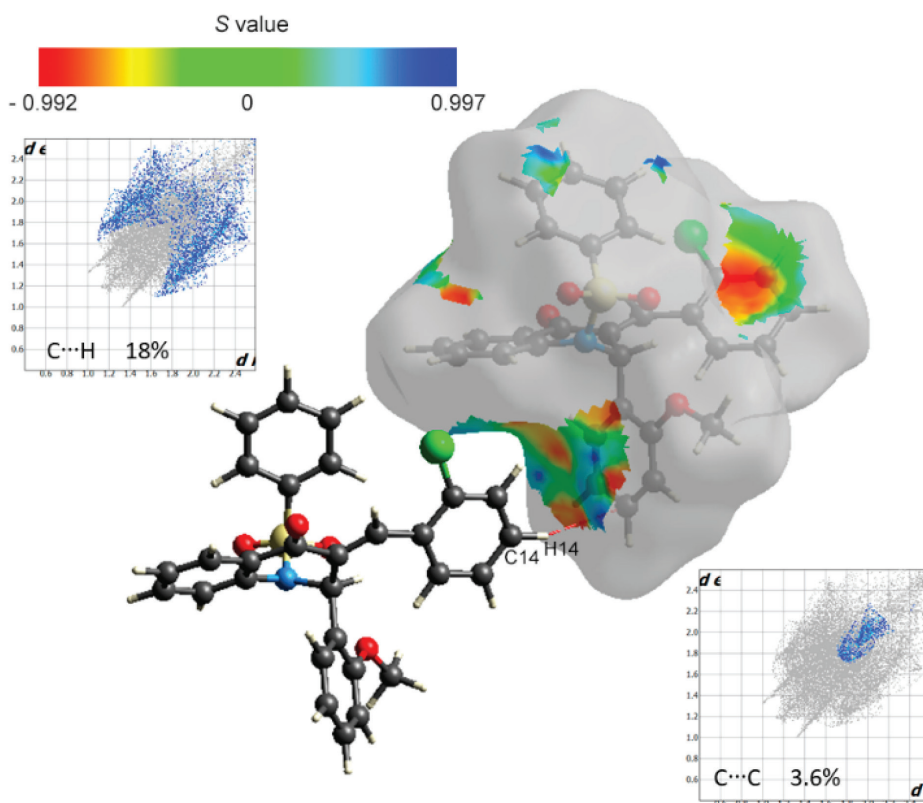
Figure 11. Hirshfield surface shape index for CMQ molecule illustrating the contact C14–H14···Cg1 and fingerprint for C···H and H···H interactions including reciprocal contacts.

asymmetrical stretching band occurs at 1325 cm⁻¹, while the symmetrical stretching band appears in the region of 1140 cm⁻¹.[29] In the title molecules, the scaled frequencies at 1299 and at 1298 cm⁻¹ have been assigned to asymmetric stretching and the scaled frequencies at 1111 and at 1113 cm⁻¹ have been assigned to symmetric stretching

mode of SO₂ group in CMQ and NMQ, respectively. In the experimental spectra, the band of asymmetric νSO_2 mode appears at 1359 and 1349 cm⁻¹, in CMQ and NMQ, respectively, while symmetric stretching vibration appears at 1165 cm⁻¹ for both compounds.

The conjugation of NO₂ group with an aromatic

Table 5. Vibrational assignments, experimental and calculated wavenumbers of CMQ (I) and NMQ (II)

Vibrational mode	Unscaled IR freq.	IR intensity / (km mol^{-1})	Scaled IR freq.[a]	IR observed / cm^{-1}
$\nu(C-C)_{Ar}$	(I) 1676-1635 (II) 1687-1638	–	(I) 1590–1551 (II) 1601-1554	(I) 1599-1463 (II) 1607-1458
$\nu(C=C)$	(I) 1710 (II) 1713	(I) 159.33 (II) 63.24	(I) 1623 (II) 1625	(I) 1599 (II) 1607
$\nu(C=O)$	(I) 1802 (II) 1806	(I) 141.65 (II) 137.65	(I) 1710 (II) 1714	(I) 1668 (II) 1676
$\nu_{asym}SO_2$	(I) 1369 (II) 1368	(I) 200.52 (II) 171.67	(I) 1299 (II) 1298	(I) 1359 (II) 1349
$\nu_{sym}SO_2$	(I) 1171 (II) 1173	(I) 172.92 (II) 179.34	(I) 1111 (II) 1113	(I) 1165 (II) 1165
$\nu_{asym}NO_2$	(II) 1703	(II) 418	(II) 1616	(II) 1525
$\nu_{sym}NO_2$	(II) 1466	(II) 197	(II) 1391	(II) 1349
$\nu(O-CH_3)$	(I) 1147 (II) 1109	(I) 56.87 (II) 33.63	(I) 1088 (II) 1052	(I) 1027 (II) 1030
$\nu(C-Cl)$	(I) 1066	(I) 47.35	(I) 1012	(I) 1027

[a]Scale factor 0.9489; ν: stretching; I: CMQ ((*E*)-3-(2-chlorobenzylidene)-2-(2-methoxyphenyl)-1-(phenylsulfonyl)-2,3-dihydroquinolin-4(1*H*)-one); II: NMQ (*E*)-2-(4-methoxyphenyl)-3-(2-nitrobenzylidene)-1-(phenylsulfonyl)-2,3-dihydroquinolin-4(1*H*)-one.

ring moves its stretch frequency in a range of 1550 to 1490 cm^{-1}, for asymmetric mode and 1355 to 1315 cm^{-1}, for symmetric mode.[41] Among the compounds present in this study, only NMQ has a nitro group present in its molecular structure. Therefore, the asymmetric stretching vibration is observed at 1525 cm^{-1} in the IR spectra and at 1616 cm^{-1} in calculated spectra. In relation to symmetric stretching vibration, it is observed at 1349 and 1391 cm^{-1} in experimental and calculated spectra, respectively. The ν(O-CH$_3$) mode appears in region[42,43] at 850 to 1100 cm^{-1}, so, in the experimental spectrum, this deformation appear in a band at 1027 cm^{-1}, for CMQ, and at 1030 cm^{-1} for NMQ. In terms of scaled frequencies, these values are at 1088 and 1052 cm^{-1}, respectively. Finally, in organic chlorine compounds, like CMQ, the ν(C–Cl) frequencies appears in the region[44] of 1129-480 cm^{-1}. In this study, this scaled frequency appears at 1012 cm^{-1}, while the experimental band appears at 1027 cm^{-1}. The graphical representation of the observed and scaled calculated spectra of CMQ and NMQ are shown in Figure 12.

The results of molecular orbital geometry and molecular electrostatic potential map calculations are presented in Figure 13. In CMQ, HOMO orbital is distributed in the region of the anisole ring, while the LUMO orbital is widely distributed by dihydroquinoline nuclei and chlorobenzene regions. For NMQ, HOMO orbital is distributed over nitrobenzene, while LUMO is dispersed over dihydroquinoline nuclei and nitrobenzene.

Using the DFT values of energy of HOMO and LUMO orbitals, some global reactivity descriptors (E$_{gap}$, hardness

and softness) were calculated.[45] In a general way, it is know that larger HOMO–LUMO energy gap indicates more stable (less reactive) compounds. This measure can also be interpreted in terms of hardness and softness, in other
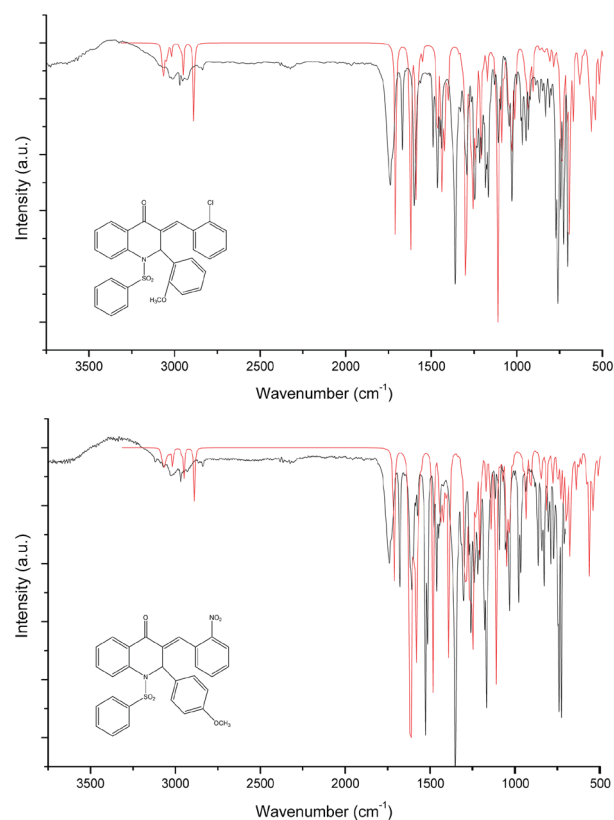
Figure 12. Overlapping of experimental (black) and scaled theoretical (red) IR spectra of CMQ (top) and NMQ (bottom).
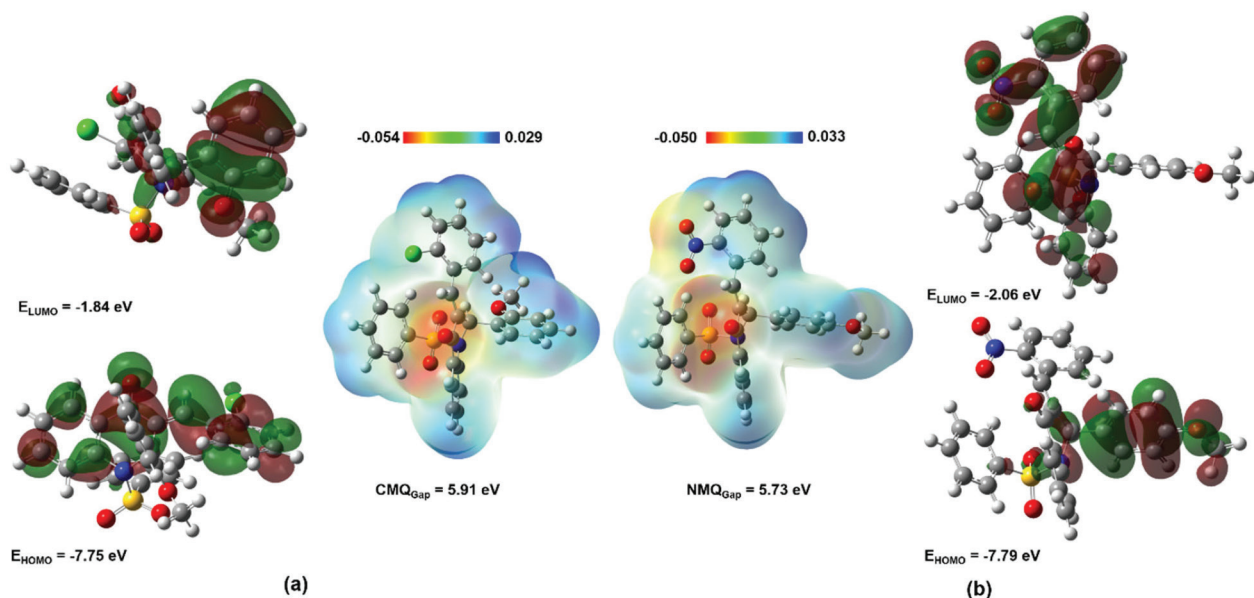
Figure 13. The HOMO, LUMO and MEP graphical representation for CMQ (a) and NMQ (b) molecules calculated using M06-2X/6-311++G(d,p) theory level.

words, the resistance of an atom to a charge transfer and the availability to receive electrons, respectively.[45-47] The calculated energies for E_{gap}, hardness and softness are, respectively: 5.91, 2.95 and 0.34 eV for CMQ and 5.73, 2.86 and 0.35 eV for NMQ. The high values of E_{gap} and hardness, when compared to NMQ, indicate that CMQ is, slightly more resistant to a charge transfer; it means, more electronic chemical stability. In relation of the capacity of both molecules to receive electrons (softness), we can expect the same behavior since the calculated values are almost equal.

The MEP analysis show high electron density sites (red regions), where are located the groups with O atoms. In CMQ, the local minimum on SO_2 group is about -0.054 a.u. That value for (C=O) group is -0.047 a.u. and for ($O–CH_3$) group is -0.041 a.u. From these results, it is possible to suggest a rank of sites that are most probable to suffer electrophiles attack as follow: SO_2 > (C=O) > ($O–CH_3$). For NMQ that rank is: SO_2 (-0.050 a.u.) > (C=O) (-0.042 a.u.) > NO_2 (-0.038 a.u.) > ($O–CH_3$) (-0.025 a.u.). On the other hand, low electron density sites (blue regions) are located at aromatic rings in both molecules. So, using the value of eletrostatic potential, it is possible to suggest a rank of sites that are most probable to suffer nucleophiles attack. That rank for CMQ is: methoxibenzene (0.027 a.u.) > cholorobenzene (0.023 a.u.) > aromatic ring at dihydroquinolin-4(1*H*)-one nucleus (0.020 a.u.). For NMQ it is: nitrobenzene (0.033 a.u.) > methoxibenzene (0.030 a.u.) > aromatic ring at dihydroquinolin-4(1*H*)-one nucleus (0.022 a.u.).

Conclusions

Both NMQ and CMQ molecules crystallized in the monoclinic space group P21/c with similar volume and density, regarding their structural similarity. It is unmistakable, for both compounds, that the most contributing intramolecular interaction is of O···H kind. Another similarity is the presence of a dimer and a C−H···π interaction. Differences can be noted in the direction of the crystal packing, probably because the substituent group chlorine in CMQ and nitro in NMQ. Furthermore, the occurrence of a non-classical π···π interaction, present in NMQ and absent in CMQ, can be explained due the nitro group acting as an stronger electron withdrawal agent than chlorine, resulting in a larger approximation of the rings. The calculated IR spectra show a good agreement between theoretical and experimental values (correlation coefficient, R^2, equal to 0.9611), so it was possible to assign the regions of absorptions of main groups in both structures. The HOMO and LUMO energies show CMQ more electronic stable than NMQ with a higher resistance to charge transfer. In addition, the regions near to O atoms have a higher electrophilic character while, aromatic rings have nucleophilic character.

Supplementary Information

^{1}H NMR, FTIR, melting point and yield of (*E*)-3-(2-nitrobenzylidene)-2-(4-methoxyphenyl)-1-(phenylsulfonyl)-2,3-dihydroquinolin-4(1*H*)-one (**5**) and (*E*)-3-(2-chlorobenzylidene)-2-(2-methoxyphenyl)-

1-(phenylsulfonyl)-2,3-dihydroquinolin-4(1*H*)-one (**6**) are available free of charge at http://jbcs.sbq.org.br as PDF file.

Acknowledgments

References

1. Nammalwar, B.; Bunce, R. A.; *Molecules* **2014**, *19*, 204.

2. Garg, M.; Chauhan, M.; Singh, P. K.; Alex, J. M.; Kumar, R.; *Eur. J. Med. Chem.* **2015**, *97*, 444.

3. Boteva, A. A.; Krasnykh, O. P.; *Chem. Heterocycl. Compd.* **2009**, *45*, 757.

4. Rodrigues-Silva, C.; Maniero, M. G.; Peres, M. S.; Guimarães, J. R.; *Quim. Nova* **2014**, *37*, 868.

5. Roussaki, M.; Hall, B.; Lima, S. C.; da Silva, A. C.; Wilkinson, S.; Detsi, A.; *Bioorg. Med. Chem. Lett.* **2013**, *23*, 6436.

6. Kwak, S. H.; Kim, M. J.; Lee, S. D.; You, H.; Kim, Y. C.; Ko, H.; *ACS Comb. Sci.* **2015**, *17*, 60.

7. Kwak, S. H.; Kang, J. A.; Kim, M.; Lee, S. D.; Park, J. H.; Park, S. G.; Ko, H.; Kim, Y. C.; *Bioorg. Med. Chem.* **2016**, *24*, 5357.

8. Sharma, K. L. N.; Kumar, C. S.; Kumaraswamy, S.; Reddy, V. K.; Rao, N. S. K.; Babu, K. R.; Ramakrishna, G.; *Tetrahedron Lett.* **2017**, *58*, 1127.

9. Nanke, Y.; Kobashigawa, T.; Yago, T.; Kawamoto, M.; Yamanaka, H.; Kotake, S.; *BioMed Res. Int.* **2016**, 6824719.

10. Kalkhambkar, R. G.; Aridoss, G.; Kulkarni, G. M.; Bapset, R. M.; Kadakol, J. C.; Premkumar, N.; Jeong, Y. T.; *Monatsh. Chem.* **2012**, *143*, 1075.

11. Vats, P.; Hadjimitova, V.; Yoncheva, K.; Kathuria, A.; Sharma, A.; Chand, K.; Duraisamy, A. J.; Sharma, A. K.; Sharma, A. K.; Saso, L.; Sharma, S. K.; *Med. Chem. Res.* **2014**, *23*, 4907.

12. Rylova, G.; Dzubak, P.; Janostakova, A.; Frydrych, I.; Konecny, P.; Holub, D.; Ozdian, T.; Dolezal, D.; Soural, M.; Hlavac, J.; Hajduch, M.; *Cancer Res.* **2012**, *72*, DOI: 10.1158/1538-7445. AM2012-4748.

13. Rylova, G.; Dzubak, P.; Janostakova, A.; Frydrych, I.; Konecny, P.; Holub, D.; Ozdian, T.; Dolezal, D.; Soural, M.; Hlavac, J.; Hajduch, M.; *Cancer Res.* **2014**, *74*, DOI: 10.1158/1538-7445. AM2014-4624.

14. Tomé, A. M.; Filipe, A.; *Drug Saf.* **2011**, *34*, 465.

15. Paramaguru, G.; Solomon, R. V.; Jagadeeswari, S.; Venuvanalingam, P.; Renganathan, R.; *Eur. J. Org. Chem.* **2014**, *2014*, 753.

16. Desiraju, G. R.; *Science* **2014**, *343*, 1057.

17. Farag, A. A. M.; Roushdy, N.; Halim, S. A.; El-Gohary, N. M.; Ibrahim, M. A.; Said, S.; *Spectrochim. Acta, Part A* **2018**, *191*, 478.

18. Bellili, A.; Pan, Y.; Al Mogren, M. M.; Lau, K. C.; Hochlaf, M.; *Spectrochim. Acta, Part A* **2016**, *164*, 1.

19. Bruker-AXS; *APEX2 Version 2014*; Wisconsin, USA, 2014.

20. Sheldrick, G. M.; *Acta Crystallogr., Sect. C: Struct. Chem.* **2015**, *71*, 3.

21. Farrugia, L. J.; *J. Appl. Crystallogr.* **2012**, *45*, 849.

22. Macrae, C. F.; Edgington, P. R.; McCabe, P.; Pidcock, E.; Shields, G. P.; Taylor, R.; Towler, M.; van de Streek, J.; *J. Appl. Crystallogr.* **2006**, *39*, 453.

23. Spek, A. L.; *J. Appl. Crystallogr.* **2003**, *36*, 7.

24. McKinnon, J. J.; Spackman, M. A.; Mitchell, A. S.; *Acta Crystallogr., Sect. B: Struct. Sci.* **2004**, *60*, 627.

25. Spackman, M. A.; McKinnon, J. J.; *CrystEngComm* **2002**, *4*, 378.

26. Wood, P. A.; McKinnon, J. J.; Parsons, S.; Pidcock, E.; Spackman, M. A.; *CrystEngComm* **2008**, *10*, 368.

27. Spackman, M. A.; Jayatilaka, D.; *CrystEngComm* **2009**, *11*, 19.

28. Chattopadhyay, B.; Mukherjee, A. K.; Narendra, N.; Hemantha, H. P.; Sureshbabu, V. V.; Helliwell, M.; Mukherjee, M.; *Cryst. Growth Des.* **2010**, *10*, 4476.

29. Frisch, M. J.; Trucks, G. W.; Schlegel, H. B.; Scuseria, G. E.; Robb, M. A.; Cheeseman, J. R.; Scalmani, G.; Barone, V.; Mennucci, B.; Petersson, G. A.; Nakatsuji, H.; Caricato, M.; Li, X.; Hratchian, H. P.; Izmaylov, A. F.; Bloino, J.; Zheng, G.; Sonnenberg, J. L.; Hada, M.; Ehara, M.; Toyota, K.; Fukuda, R.; Hasegawa, J.; Ishida, M.; Nakajima, T.; Honda, Y.; Kitao, O.; Nakai, H.; Vreven, T.; Montgomery Jr., J. A.; Peralta, J. E.; Ogliaro, F.; Bearpark, M.; Heyd, J. J.; Brothers, E.; Kudin, K. N.; Staroverov, V. N.; Kobayashi, R.; Normand, J.; Raghavachari, K.; Rendell, A.; Burant, J. C.; Iyengar, S. S.; Tomasi, J.; Cossi, M.; Rega, N.; Millam, J. M.; Klene, M.; Knox, J. E.; Cross, J. B.; Bakken, V.; Adamo, C.; Jaramillo, J.; Gomperts, R.; Stratmann, R. E.; Yazyev, O.; Austin, A. J.; Cammi, R.; Pomelli, C.; Ochterski, J. W.; Martin, R. L.; Morokuma, K.; Zakrzewski, V. G.; Voth, G. A.; Salvador, P.; Dannenberg, J. J.; Dapprich, S.; Daniels, A. D.; Farkas, Ö.; Foresman, J. B.; Ortiz, J. V; Cioslowski, J.; Fox, D. J.; *Gaussian 09, Revision A.02*; Gaussian Inc., Wallingford CT, 2009.

30. Seifert, N. A.; Steber, A. L.; Neill, J. L.; Pérez, C.; Zaleski, D. P.; Pate, B. H.; Lesarri, A.; *Phys. Chem. Chem. Phys.* **2013**, *15*, 11468.

31. Michelini, L. J.; Castro, M. R. C.; Custodio, J. M. F.; Naves, L. F. N.; Vaz, W. F.; Lobón, G. S.; Martins, F. T.; Perez, C. N.; Napolitano, H. B.; *J. Mol. Struct.* **2018**, *1168*, 309.

32. Singh, S. K.; Joshi, P. R.; Shaw, R. A.; Hill, J. G.; Das, A.; *Phys. Chem. Chem. Phys.* **2018**, *20*, 18361.

33. Garnica, M. M.; Torres, A. E.; Ramírez-Caballero, G. E.; Balbuena, P. B.; *Microporous Mesoporous Mater.* **2018**, *265*, 241.

34. Zhao, Y.; Truhlar, D. G.; *Theor. Chem. Acc.* **2008**, *120*, 215.

35. Sert, Y.; Ucun, F.; El-Hiti, G. A.; Smith, K.; Hegazy, A. S.; *J. Spectrosc.* **2016**, *2016*, 1.

36. James, W. H.; Buchanan, E. G.; Müller, C. W.; Dean, J. C.; Kosenkov, D.; Slipchenko, L. V.; Guo, L.; Reidenbach, A. G.; Gellman, S. H.; Zwier, T. S.; *J. Phys. Chem. A* **2011**, *115*, 13783.

37. Jamroz, M. H.; *Vibrational Energy Distribution Analysis VEDA 4*; Warsaw, Poland, 2004.

38. Dennington, R.; Keith, T.; Millam, J.; *GaussView*, version 5; Semichem Inc., Shawnee Mission, Kansas, 2009.

39. Alecu, I. M.; Zheng, J.; Zhao, Y.; Truhlar, D. G.; *J. Chem. Theory Comput.* **2010**, *6*, 2872.

40. Custodio, J. M. F.; Faria, E. C. M.; Sallum, L. O.; Duarte, V. S.; Vaz, W. F.; de Aquino, G. L. B.; Carvalho Jr., P. S.; Napolitano, H. B.; *J. Braz. Chem. Soc.* **2017**, *28*, 2180.

41. Pavia, D. L.; Lampman, G. M.; Kriz, G. S.; Vyvyan, J. A.; *Introduction to Spectroscopy*, 5th ed.; Cengage Learning: Mason, Ohio, USA, 2015.

42. Raj, A.; Raju, K.; Varghese, H. T.; Granadeiro, C. M.; Nogueira, H. I. S.; Panicker, C. Y. Y.; *J. Braz. Chem. Soc.* **2009**, *20*, 549.

43. Panicker, C. Y.; Varghese, H. T.; John, M. A.; Harikumar, B.; *Orient. J. Chem.* **2008**, *24*, 973.

44. Mooney, E. F.; *Spectrochim. Acta* **1964**, *20*, 1021.

45. Ramaganthan, B.; Gopiraman, M.; Olasunkanmi, L. O.; Kabanda, M. M.; Yesudass, S.; Bahadur, I.; Adekunle, A. S.; Obot, I. B.; Ebenso, E. E.; *RSC Adv.* **2015**, *5*, 76675.

46. Sklenar, H.; Jäger, J.; *Int. J. Quantum Chem.* **1979**, *16*, 467.

47. Karthiga Devi, P.; Venkatachalam, K.; *J. Mater. Sci.: Mater. Electron.* **2016**, *27*, 8590.